Egypt. J. Chem. **Vol. 64,** No. 5 pp. 2315 - 2324 (2021)

Egyptian Journal of Chemistry

http://ejchem.journals.ekb.eg/

Synthesis and Characterization of Polymer Supported Organoclay Nanoparticles

Magda A Akl* and Mohammed A Ibraheim

Department of Chemistry, Faculty of Science, Mansoura University, Mansoura 35516, Egypt

Abstract

Octadecylamine modified montomorillonite/poly(styrene-co-acrylamide) (Oct-MMT/PSTAM) nanogels with unique morphologies of core/shell and core/shell/shell structures were fabricated. The transmission electron microscopy (TEM) images of The as-prepared composites revealed the formation of double and triple coated structures with average size of 152 nm and 52 nm, respectively. New nanocomposites (MHs(1-3)) were fabricated by impregnating Oct-MMT/PSTAM latex with core/shell/shell structure onto crosslinked poly(sodium acrylate-co-acrylamide) (PSAAM) of various molar ratio. PSAAM was selected as a support material because it has a higher swelling ratio and will achieve an expected compatibility with MMT/PSTAM nanogel. These MHs nanocomposites were characterized by Fourier transform infrared spectroscopy (FTIR), scanning electron microscopy (SEM), X-ray diffraction (XRD), X-ray fluorescence (XRF) and differential scanning calorimetry (DSC).

Keywords: Montomorillonite, Octadecylamine, XRD, FTIR, TEM, DSC.

1. Introduction

Core-shell polymers (CSPs) are structured composite particles consisting of at least two different components, one in principle forms the core and another forms the shell of the particles. [1-3] This class of materials has attracted much attention because of the combination of superior properties not possessed by the individual components. The systems might combine the characteristics and properties of both shell and core where the surface properties of the shell are translated to the core, imparting new functionality to the CSP [4, 5]. CSPs have been used in a number of applications such pollution control [6-12].

Polymer-nanoclay composites have attracted considerable attention due to their unique properties and broad applications [13-19]. The polymer/layered phyllosilicate nanocomposite was developed based on evenly dispersing the clay into a polymer matrix by simple mechanical mixing, melt or bulk polymerization, solution polymerization, and emulsion or suspension polymerization approaches[20,21]. Among the approaches mentioned above, the product in aqueous form has unique advantages, because of the ease of manipulation, low cost, and absence of environmental concerns. Several researchers [22-24] have attempted to synthesize polymer encapsulated nanoclay composite via suspension, emulsion or miniemulsion polymerization methods. Xu et al. [21] described a method to synthesize intercalated poly (styrene-co- methyl methacrylate) clay nanocomposites through an emulsion polymerization by using a reactive surfactant, 2-acrylamido-2-methyl-1-propane sulphonic acid (AMPS). Huang et al. [22] prepared a polymer/clay nanocomposite by suspension polymerization of MMA with montmorillonite. However, the product obtained was not in a thermodynamically stable water dispersion form. The nanocomposite they prepared through emulsion polymerization was a simple process of mixing clay with as-prepared emulsion latex of PMMA. No substantial encapsulation was observed. Kim and co-workers [20, 24] synthesized a styrene-acrylonitrile (SAN) copolymer-clay nanocomposite using a conventional emulsion polymerization and observed typical electrorheological (ER) behavior from the ER fluid composed of intercalated particles and silicon oil. However, the product they obtained was in a coagulated form. Herrera et al. [23] synthesized the water-based polymer clay nanocomposites by first

*Corresponding author e-mail : magdaakl@yahoo.com .; (Prof Magda A Akl).
Receive Date: 13 January 2021, Revise Date: 02 February 2021, Accept Date: 16 February 2021
DOI: 10.21608/EJCHEM.2021.57889.3244

chemically modifying the laponite clay minerals by silane agents (γ-methacryloxy propyl mono-, di-, trimethyl ethoxysilane) before the polymerization and then proceeding with seeded emulsion polymerization. However, the stability of the final latex was not reported.

To date, to the best of our knowledge, all the previous attempts of preparation include encapsulation of nanoclays within the polymer matrix to obtain either an exfoliated or intercalated structures. There is no report till now deals with preparation of polymer-nanoclay composites with core/shell/shell morphology. Our focus in this area is to use simple methodology to prepare water dispersible stable colloid of octadecylamine modified montomorillonite/poly(styrene-co-acrylamide) nanogels with unprecedented double and triple coat morphology. Moreover, these nanogels are used as fillers to prepare efficient supersorbent composites. The preparation and characterization of all materials are highlighted in this article.

2. Experimental

2.1. Materials

Styrene (St), Acrylamide (AM), acrylic acid (AA), 2-Hydroxyethyl methacrylate (HEMA), Polyvinyl pyrolidone (PVP), N,N`- methylenebisacrylamide (MBA) and Surface modified montomorillonite nanoclay containing 25 – 35 % octadecylamine (Oct-MMT) were purchased from Sigma Chemical Co. Styrene was purified by washing with 5 wt.% NaOH solution followed by deionized water until a pH of 7 was reached, all other reagents were used as received. The initiator potassium peroxodisulfate (KPS) and the accelerator N,N,N′,N′-tetramethyl ethylene diamine (TEMED) were provided by Merck and used as received.

Sodium acrylate monomer (AA-Na) was prepared as follows. An amount of 12.01 g (0.3003 mol) of NaOH and 10 mL of water were mixed with a magnetic stirring bar, and the mixture was stirred to dissolution. NaOH solution was carefully added to a 250 mL beaker containing 28.03 g (0.3893 mol) of AA (exothermic reaction), with continuous stirring. The mixture was allowed to cool, 50 mL of acetone was added and the precipitate was vacuum-filtered. The wet AA-Na was first air- dried and subsequently dried in an oven at 60 ◦C for 12–15 h to obtain 27.31 g (96.8% yield) of AA-Na.

2.2. Synthesis of octadecylamine modified montomorillonite / poly(styrene-co-acrylamide) latex particles

Oct-MMT/PSTAM nanocomposite latex was prepared via free radical copolymerization of styrene and acrylamide in the presence of Oct-MMT as seed nanoparticles and polyvinyl pyrolidone as a stabilizer. In a typical experiment, 0.025 g Oct-MMT were dispersed in 50 mL EtOH/H2O (60/40 v/v) then 0.025 g PVP was added to the mixture under vigorous stirring. After that, 1.48 mL styrene and 1.01 g acrylamide were charged to the reaction mixture followed by bubbling with nitrogen. The reaction mixture was maintained at room temperature by circulating water bath. KPS initiator (1% with respect to total monomers mass) dissolved in 3 mL H2O and added to the reaction vessel. Finally, 25 µL TEMED was added to start the polymerization process. The reaction mixture stirred for 24 h. at room temperature, this sample takes the designation (MA1). Another two samples namely MA2 and MA3 were prepared with the same procedure but 0.05 g Oct-MMT was used instead of 0.025 g Oct-MMT for MA2 sample and HEMA instead of Styrene.

2.3. Synthesis of polymer supported Oct-MMT/PSTAM nanocomposites

A series of nanocomposite hydrogels were prepared via free radical polymerization of sodium acrylate and acrylamide in the presence of fixed amount of Oct-MMT/PSTAM nanogel (sample MA2). The total monomer concentration kept constant (30 wt %) while AM/AA-Na molar ratio was varied 90/10, 50/50 and 10/90 to get MH1, MH2 and MH3 samples, respectively. In the preparation of samples, AM, AA-Na, MBA, and clay nanogel were dissolved in water in an ice cooled bath. Prior to the polymerization, dried nitrogen was bubbled into the mixture. Potassium persulfate (1% with respect to monomer mass) and TEMED were added into the mixture as an initiator and activator, respectively. Unreacted monomers were removed from the samples by keeping the discs in distilled water. Then the hydrogel samples were filtered and dried under vacuum at 50°C to obtain powder samples.

2.4. Characterization

FTIR spectra were analyzed with a Nicolet FTIR spectrophotometer using KBr in a wavenumber range of 4000–500 cm^{-1} with a resolution accuracy of 4 cm^{-1}. All samples were ground and mixed with KBr and then pressed to form pellets. High resolution transmission electron microscopy (HR-TEM) images for these nanocomposites were recorded using (JEM-2100F, JEOL, Japan) at an acceleration voltage of 150 kV. X-ray diffraction measurements of nanocomposites were carried out using a JOEL JDX-3530 diffractometer (Cu Kα radiation, λ=0.15405 nm, 2 kW). Low angle and wide angle X-ray diffraction (XRD) patterns were recorded at a scanning rate of 0.02° min^{-1}. The d (001) basal spacing of the original clay and the exfoliated clay were calculated using the Bragg equation: $d=\lambda/2\sin\theta$

The surface morphologies of MH1, MH2 and MH3 nanocomposites were investigated using scanning

electron microscopy (SEM, model JSM-T 220A, JEOL, Japan) at an accelerated voltage 20 kv. The chemical compositions of nanocomposite particles were determined using energy dispersive X-ray fluorescence spectrophotometer (Rigaku NEX CG). DSC characterization was performed using Differential Scanning Calorimeter (DSC-50 Shimadzu) instrument. Approximately 10 mg of finely ground sample was heated in a corundum crucible with a heating rate of 10◦C/min under air atmosphere.

3. Results and discussion

The preparation of nanocomposites requires extensive delamination of the layered clay structure and complete dispersion of the resulting platelets throughout the polymer matrix. Nanocomposite synthesis by conventional polymer processing operations therefore requires strong interfacial interaction between the polymer matrix and the clay [25]. For achieving this purpose we demonstrate using hydrophobic nanoclay (Oct-MMT) as a core while acrylamide and styrene were used as monomers for construction of polymeric shell. The hydrophobicity of styrene monomer favors its retention within the intergalleries of the clay and exfoliates the clay from a stacked architecture to an individually dispersed platelet form after polymerization. The polarity and hydrogen bonding capacity of acrylamide generates considerable adhesion between the polymer and the clay phase. Meanwhile, a complete encapsulation of Oct-MMT within the polymeric shell could be achieved via polymerization of monomers in the presence of H_2O/EtOH dispersion of Oct-MMT using PVP as a stabilizer. PVP not only act as a stabilizer but also participates in the exfoliation process

3.1. Transmission electron microscopy(TEM)

TEM provides the best proof for encapsulation of Oct-MMT within poly(styrene-co-acrylamide). TEM images of MA1, MA2 and MA3 latex particles are shown in Figures 1-3, respectively. TEM image of MA1 sample (Figure 1) discloses successful preparation of core shell structure with will defined spherical morphology. The poly(styrene-co-acrylamide) shell completely surround the organoclay core and the particle size was estimated to be 152 nm. TEM images of Oct-MMT/PSTAM prepared using high content of clay nanoparticles (sample MA2) reveal a dramatic change in morphology (Figure (2a, b)). It is clearly noticed that a triple coat structure is formed with average size 52 nm. High magnification image (Figure 2b) contains a dark central zone, a dark outer shell and white circle in between the central zone and outer shell. The dark zones represent the clay nanoparticles while the white coat represents poly(styrene-co-acrylamide) shell since the inorganic constituents of clay nanoparticles scatter the electron beam more effectively than the polymeric shell leading to appearance of dark zones. This behavior can be attributed to dislocations of organoclay galleries from each other and formation of bilayer via hydrophobe hydrophobe interaction between octadecylamine attached to montomorillonite. Due to the structure affinity between styrene monomers and hydrophobic chains of octadecylamine, styrene monomers entered into the core of bilayer while the backbone of montomorillonite is directed toward the continuous phase because of high polarity of silicate platelets. In this morphology, the organoclay act as stabilizer for poly(styrene-co-acrylamide) since the concentration of organoclay is sufficient to form inner core and outer shell. López-López et al. [26] used organo-clay derived from bentonite and modified with tetraalkylammonium cations to stabilize magnetorheological fluids constituted of micrometer sized particles dispersed in kerosene but SEM images indicated formation of big aggregates of clay without any distinct features about formation of core shell or core/shell/shell structures. The key parameter in formation of bilayer and appearance of core/shell/shell morphology is prolonged stirring of Oct-MMT in H_2O/EtOH mixed solvent system prior to polymerization process. The nanoscale platelets of montomorillonite are made of two dimensional 1 nm layers of an aluminate sheets sandwiched between two silicate sheets [27]. The layers are stacked together by weak ionic and Van der Waals forces. Under vigorous stirring, the layers can be completely separated and reorientation occurs to reach stability by formation of double sheath of Oct-MMT. TEM images of Oct-MMT / poly(Acm-co-HEMA) nanohybride (Figure (3a,b)) indicate that, core shell nanohybride containing several number of clay nanoparticles in the core is formed. The polymeric shell, which is insufficient to cover the total surface area of the primary clay particles, redistributed onto the reduced surface area of the aggregates and prevents further agglomeration. The average particle width and length of irregular sphere was estimated to be 150 nm and 350 nm, respectively. Figure 4a shows that EtOH/H_2O compromises an excellent mixed solvent for successful preparation of stable nanocomposite latex particles. The colloidal stability of MA1 and MA2 nanogels (Figure 4b and Figure 4c, respectively) can be attributed to steric repulsion provided by PVP.

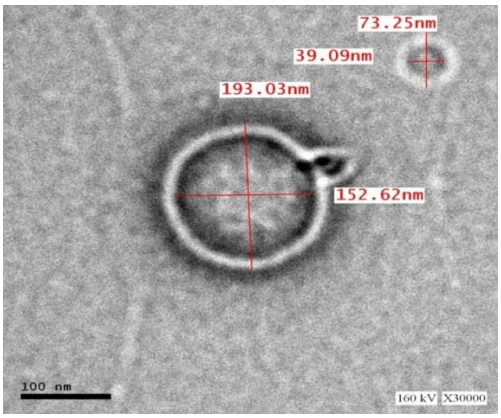

Figure 1: TEM images of Oct-MMT/PSTAM latex particles (MA1 sample) prepared using low content of Oct-MMT

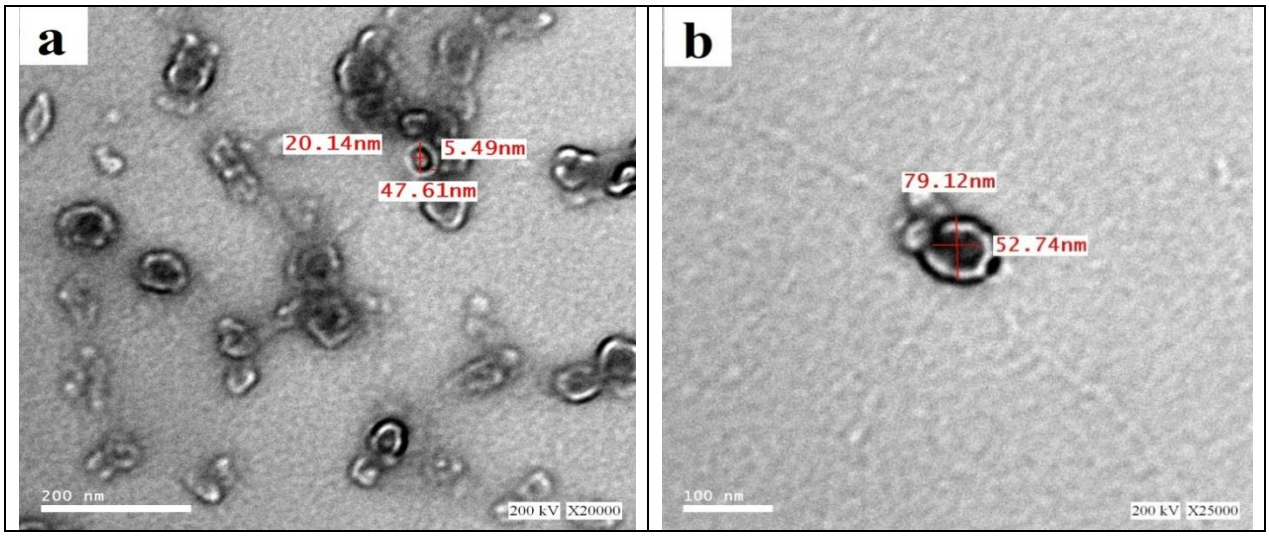

Figure 2: TEM images of Oct-MMT/PSTAM latex particles (MA2 sample) prepared using high content of Oct-MMT at two different magnifications (a) 20000 and (b) 25000.

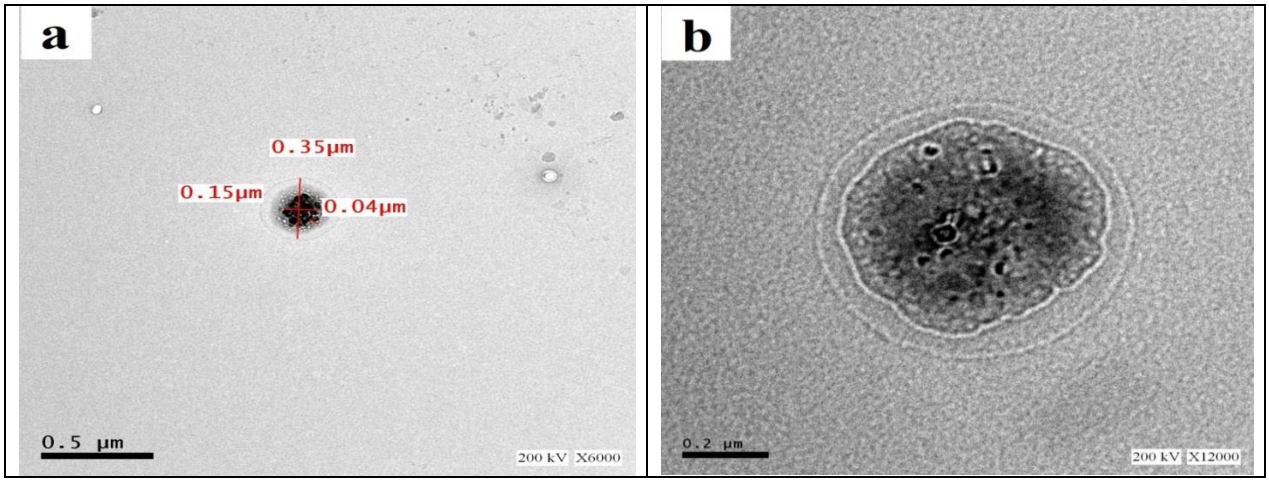

Figure 3: TEM images of MA3 nanohybride at two different magnifications (a) 6000 and (b) 12000.

Figure 4: Photographic images of (a) dispersion of Oct-MMT in EtOH/H_2O mixture in the presence of PVP. Colloidal stability of Oct-MMT/PSTAM latex particles prepared using: (b) low clay content (MA1 sample), (c) high clay content (MA2 sample).

3.2. FTIR characterization

The FTIR spectra of organic montomorillonite and the as prepared MHs oganoclay nanocomposites, were performed in the range of 4000-400 cm^{-1} and compared with each other to obtain information on the immobilization of polymer between layers of montomorillonite. Figure 5a shows the FTIR spectrum of the organic montomorillonite sample. The bands at 465 and 527 cm^{-1} are corresponded to Si-O-Si and Al-O-Si bending vibrations[28, 29]. The band at 634 cm^{-1} is assigned to the out-of-plane vibrations of coupled Al-O and Si-O. The band at 848 cm^{-1} is assigned to the bending vibration of Al-Mg-OH. The spectral band at 919 cm^{-1} reflects the stretching vibration of Al-O-(OH)-Al [30-34]. The strong band at 1038 cm^{-1} represents the Si-O-Si groups of the tetrahedral sheet. The spectral band at 1648 cm^{-1} reflects the bending of H-OH bond of water molecules, which is retained in the matrix. The peaks at 2854 and 2925 cm^{-1} are assigned to the aliphatic C-H stretching vibration of the methylene and methyl group CH_2, CH_3 of the aliphatic chain of octadecyl amine. Also, C-H in plane bending vibration of the methylene groups can be seen at wavelength bands of 1477 cm^{-1}, verifying the intercalation of surfactant molecules between the silica layers. The broad band at 3436 cm^{-1} is due to H-OH stretching vibration of the water molecules adsorbed on the solid surface. The strong band at 3637 cm^{-1} attributed to O-H stretching vibration of the silanol (Si-OH) groups from the solid (OH groups between octahedral and tetrahedral sheets) and Al(Mg)–O–H stretching vibration. The absorption band at 3246 cm^{-1} is related to N-H stretching vibration of amino group of octadecylamine.

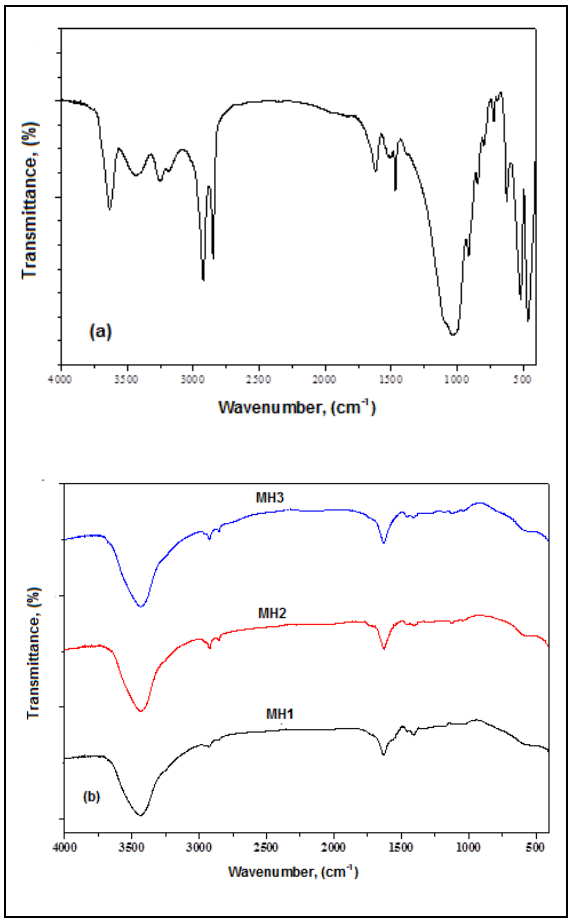

Figure 5: FTIR spectrum of (a) Oct-MMT and (b) MH1, MH2 and MH3 nanocomposite

FTIR spectra of MH1, MH2 and MH3 nanocomposite hydrogels are shown in Figure 5b. The FTIR spectra of nanocomposite hydrogels showed additional bands with respect to the FTIR spectrum of organic montomorillonite, FTIR spectrum of MH1 shows a strong band at 3436 cm^{-1} which is assigned to COOH group of sodium acrylate and O-H stretching vibration of the silanol (Si-OH) groups from the solid. The absorption peaks originating from the C=O group at 1649 cm^{-1} and NH

bending vibration at 1548 cm^{-1} of the acrylamide unit can be seen. Small shoulder at 3263 cm^{-1} belongs to NH_2 stretching vibration of acrylamide. The bands in the range: 1400-1600 cm^{-1} are responsible for the benzene ring vibrations of styrene. However, these bands have lower intensity and are not well resolved. It is probably the result of phenyl ring π electrons interaction with the π electrons of the oxygen planes of montomorillonite layers. On the other hand, absorption peak at 3637 cm^{-1} which correspond to the OH groups in clay structure disappeared. Based on these results, it is supposed that the grafting mechanism was occurred on the clay layers. This phenomenon was explained by several researchers before [35, 36]. When the clay was modified by polymer the O–H band of silicate at 3436 cm^{-1} became broader, and shifted to 3434 cm^{-1}.These results clearly show that high interfacial interactions existed between the clay layers and polymer matrix and a hydrogel/clay nanocomposite structure was obtained by in situ copolymerization. It is difficult to determine the type of interaction occurring between clay and polymer by FT-IR. Only a small amount of clay is present in the nanocomposites. Furthermore, Na-MMT itself has a complicated FT-IR spectrum. Consequently, overlapping between bands originating from both clay and polymer makes it very difficult to detect characteristic shift in bands of clay in the presence of acrylamide and sodium acrylate. However, FT-IR at least confirms the presence of interaction between polymer and clay. FTIR spectra of MH2 and MH3 are similar to that of MH1 and no significant differences were noticed except for the band at 3436 cm^{-1}. For MH2 and MH3, this band is located at 3432 and 3430 cm^{-1}, respectively. This behavior attributed to the increase in interaction between montomorillonite and the polymer with increasing the acrylamide content.

3.3. Scanning electron microscopy (SEM)

The Morphologies of the as-prepared MH1, MH2 and MH3 nanocomposites were investigated using SEM (Figure (6a-f)). The samples were dried at 60 °C in vacuum oven. This process removes water and would have caused some collapse of the hydrated structures initially present. From Figure 6(a,b), it could be clearly seen that MH1 and MH2 nanocomposites had large numbers of pores. The pore sizes of MH2 was smaller than these of MH1 nanocomposite, supporting the fact that the MH2 nanocomposite hydrogel had a lower swelling ratio due to the correlation between water content and pore size (i.e., the higher the water content of swelled hydrogel, the bigger the pore size of freeze-dried gels). In addition, the pores of MH2 nanocomposite are regular with well-shaped sphere than that of MH1 nanocomosite, suggesting that the MH2 nanocomosite had a well-defined polymer network. Usually, the well-defined network can evenly distribute the stress into the polymer matrix [37], thereby improving the mechanical properties of hydrogel. Figure 6(d,e) show the SEM images of MH1 and MH2 nanocomposites at the high magnification level. Interestingly, a few amount of montomorillonite were visible in the cavities of the pores (indicated by the arrows). Also, the average pore diameter of MH 1 and MH2 nanocomposites are 365 and 71.5 nm, respectively. In all samples, the clay was buried deep inside the polymer matrix and whether the nanocomposites are exfoliated or intercalated can't be determined using SEM. SEM micrographs of MH3 nanocomposite are shown in Figure 6(c,f). Interestingly, it could be clearly seen that sheets are evident and there is no pores on the surface. The edges of the sheets can be seen, and it is suggested that they have a nanometer thickness. These sheet morphologies appear to be rather smooth and are unprecedented for montomorillonite/polymer mixtures to our knowledge.

.

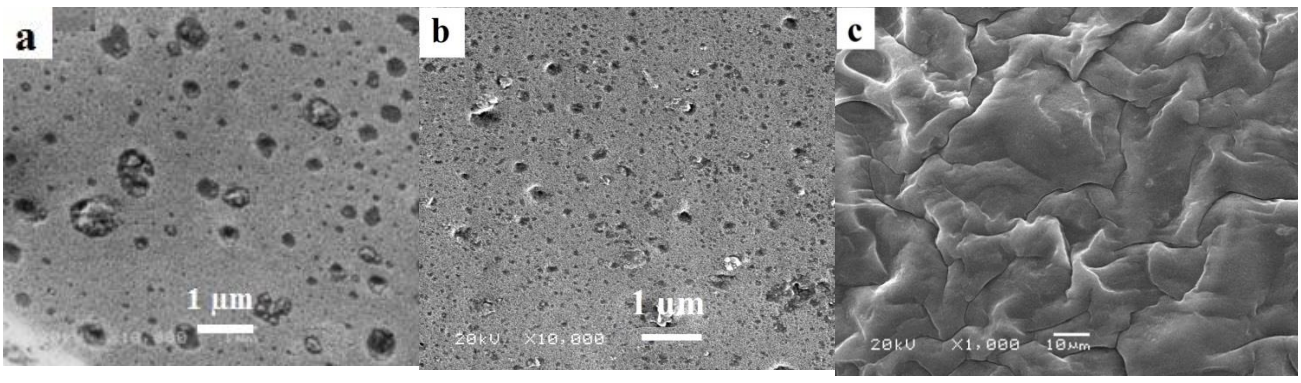

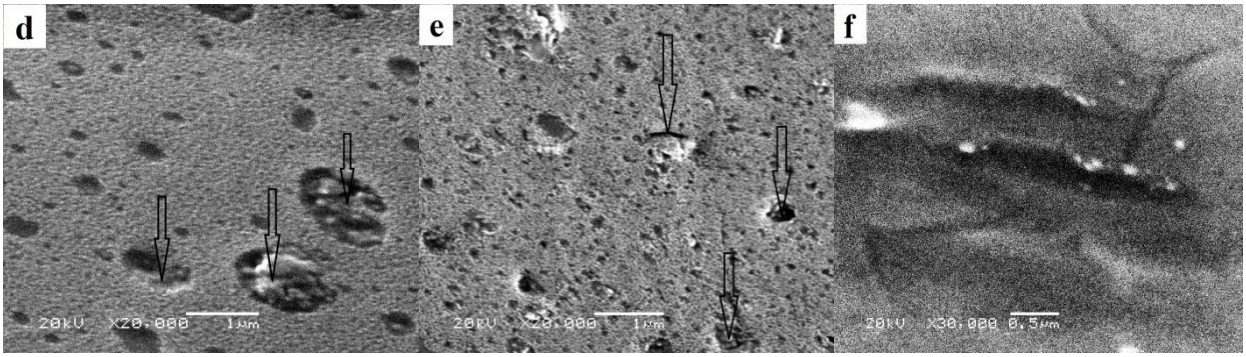

Figure 6: SEM images of MH1, MH2 and MH3 nanocomposite hydrogels at two different magnifications: (a) MH1 at 10000, (b) MH2 at 10000, (c)) MH3 at 1000, (d)) MH1 at 20000, (e) MH2 at 20000 and (f) MH3 at 30000.

3.4. Wide Angle X-ray diffraction

Low angle and wide angle X-ray diffraction of organically modified montomorillonite are shown in Figure 7(a & b), respectively. The inorganic atoms (Al or Mg) scatter the incident beam (X-ray) to give a regular pattern of arrangements. The separation (d) between the individual silicate layers is obtained from Bragg's equation,

$$n\lambda = 2d \sin 2\theta \quad (1)$$

where n is the order of the reflection, λ is the wavelength of the incident X-ray beam, d is the spacing between multilayers, and is the angle X-ray beam and the plane of multilayers. Non modified montomorillonite shows a basal spacing of 12.74 °A [38]. After the modification process, this basal spacing increased to 21.5 °A. With the insertion of octadecylamine into the montomorillonite interlayer, the clay became hydrophobic; improving its organic adsorption capacity. WAXD of MH1, MH2 and MH3 nanocomposite hydrogels are shown in Figure 8(a-c), respectively. By monitoring the position, shape, and intensity of the basal reflections from the distributed silicate layers, the polymer clay structure, either intercalated or exfoliated, may be identified. In case of exfoliated nanocomposites, the extensive layer separation associated with the delamination of the original silicate layers in the polymer matrix results in the eventual disappearance of any coherent X-ray diffraction from the distributed silicate layers. On the other hand, when intercalation occurs, in which well-ordered multilayered structures exist, the reflection peak shifts toward a lower 2θ value, indicating finite layer spacing expansion. Peak broadening and intensity loss is typical for the disordered intercalated system.

The X-ray diffraction patterns of MH1 and MH2 nanocomposites (Figures 8(a,b)) have no Bragg diffraction peaks and there is no distinctive reflection peak and featureless spectra are obtained, indicating that the clay has been completely exfoliated or delaminated in the polymer matrix. For MH3 nanocomposite (Figure 8(c)), the absence of WAXD at low angle area and appearance of non-characteristic peaks at $2\theta = 31.6^{\circ}$ and 45.3° indicates that the nanocomposite has exfoliated structure. The exfoliated structure in all samples attributed to: (1) the structure affinity between styrene monomer and the octadecylamine of organic clay. (2) The nature of solvent which facilitate insertion of monomers between silicate layers and enhance swelling of organoclay. (3) Rate of stirring which destroy the tactoid structure and separate silicate layers from each other. (4) The amido groups of acrylamide co-monomer can form hydrogen bonds with water molecules surrounding the inorganic exchangeable cations. The presence of broad peaks in all samples attributed to the amorphous nature of polymer**.**

3.5. X-ray Flourescence

The chemical composition of Oct-MMT nanoparticles obtained by using XRF analysis is given in table 13. The results indicate that, Oct-MMT consists of silica and alumina as major constituents along with traces of potassium, iron, sulfur, calcium, and titanium oxides in the form of impurities. Also, it is expected that the prepared nanocomposites will have efficient adsorption power toward toxic metals since the adsorbate species will be removed mainly by SiO_2 and Al_2O_3.

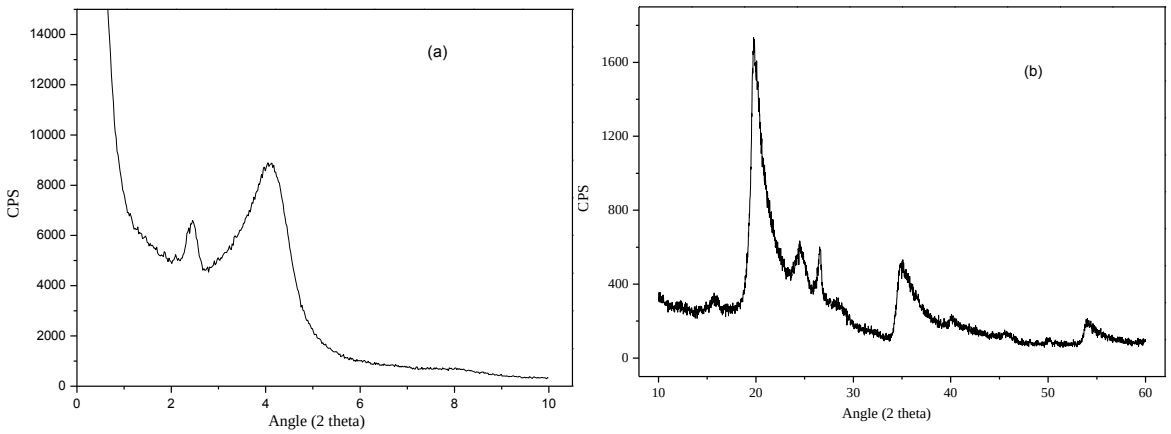

Figure 7: (a) Low angle X-ray diffraction pattern and (b) WAXRD of Oct-MMT

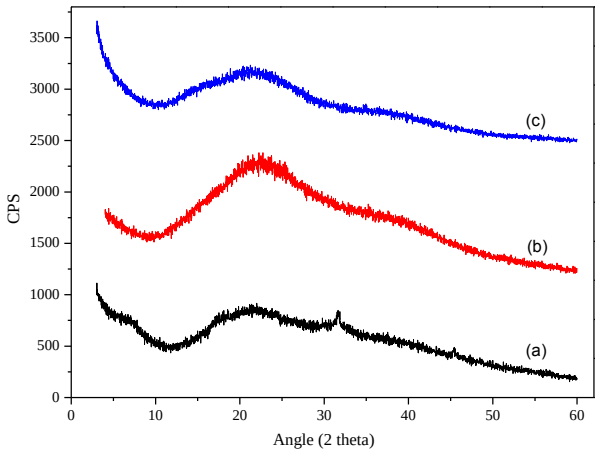

Figure 8: XRD diffraction patterns of MH1, MH2 and MH3 nanocomposites

Table 1 XRF of organic montomorillonite nanoparticles and MA 1, MA 2 and MA 3 nanocomposites

Oxide	Organoclay Wt%	Element	MA 1 Wt%	MA 2 Wt%	MA 3 Wt%
MgO	ND	Mg	0.244	ND	ND
Al_2O_3	21.6	Al	ND	0.0227	0.0409
SiO_2	72.5	Si	0.0649	0.0615	0.0805
P_2O_5	0.0486	P	ND	0.0005	ND
SO_3	0.408	S	0.0036	0.0043	0.0046
Cl	0.541	Cl	0.116	0.0293	0.0332
K_2O	0.347	K	0.0982	0.101	0.0962
CaO	0.101	Ca	0.0194	0.0216	0.0289
TiO_2	0.502	Ti	0.0007	0.0007	0.0009
V_2O_5	0.0248	V	0.0001	0.0001	ND
Cr_2O_3	0.0033	Cr	0.0001	0.0001	0.0001
MnO	0.0099	Mn	ND	ND	0.0003
Fe_2O_3	3.78	Fe	0.0050	0.0051	0.0071
Co_2O_3	0.0188	Co	ND	ND	ND
NiO	0.0045	Ni	0.0002	0.0002	0.0002
CuO	0.0022	Cu	0.0010	0.0004	0.0006

ZnO	0.0286	Zn	0.0010	0.0005	0.0009
Ga_2O_3	0.0063	Ga	ND	ND	ND
As_2O_3	0.0007	As	ND	<0.0001	ND
SeO_2	0.0003	Br	0.0001	<0.0001	0.0001
Br	0.0021	Rb	<0.0001	ND	0.0001
Rb_2O	0.0028	Sr	0.0001	0.0001	0.0002
SrO	0.0082	Cd	ND	0.0004	ND
Y_2O_3	0.0046	Sn	0.0021	0.0013	0.0022
Nb_2O_5	0.0026	Te	ND	ND	ND
SnO_2	0.0025	Hf	0.0001	ND	0.0002
HfO_2	0.0030	Ta	ND	ND	ND
Ta_2O_5	0.0024	Ir	ND	0.0001	ND
Ir_2O_3	0.0017	Au	<0.0001	ND	ND
PtO_2	0.0013	Pb	0.0002	0.0005	0.0003
Au2O	0.0013	PP	99.43	99.75	99.56
Tl_2O_3	0.0013				
PbO	0.0035				
ThO_2	0.0080				
U_3O_8	0.0028				

3.6. Differential Scanning Calorimetry

In order to know the influence of polymer structure on flexibility of polymer chains, the glass transition temperature (Tg) was determined from DSC measurements [39] as indicated in experimental section. Tg value obtained from DSC scans for MH1, MH2 and MH3 nanocomposite. From data obtained it was obvious that, the nanocomposites show a single Tg, indicating the compatibilities between clay nanogel and polymer matrix. Also, the results clearly indicate that Tg values of nanocomposites depends on the composition of comonomers and it increases with increasing acrylamide content in the nanocomposite. The relative high Tg value of MH3 nanocomposite (61.3 °C) are due to the interaction between amide group and carboxylic group attached to the backbone of the polymer. This interaction facilitated entanglement of polymer chains and it can also be associated with a lower free volume mobility and flexibility than MH1 and MH2 nanocomposites. The high Tg value may be also due to decrease in the segmental mobility of polymer chains as a result of anchoring of hydrogen bonding between the chains. Moreover, the higher Tg value were revealed to the interaction between amino group and silicate layers of montomorillonite. In contrast, MH 1 nanocomposite has lower Tg value (54.9 °C) compared to MH2 (56.6 °C) and MH3 (61.3 °C) due to decreasing the interaction between the polymer chains with decreasing amount of acrylamide co-monomer. Also, introducing a small amount of water to a hydrophilic polymer may disrupt the intermolecular bonds, thereby enhancing the main-chain motion. In this case Tg shifts to lower temperatures in the presence of water, indicating the higher swelling ratio of MH1than MH2 and MH3. Hydrophilic polymers stored under ambient conditions contain a certain amount of bound water [40].

Conclusion

In the present study, we reported the preparation of core /shell and core/shell/ shell polymer supported orgnoclay nanocomposites. These as prepared nanocomposites were characterized using TEM, SEM, FTIR and XDR. In order to know the influence of polymer structure on flexibility of polymer chains, the glass transition temperature (T_g) was determined from DSC measurements The observed properties of the as prepared(Oct-MMT/PSTAM) nanocomposites encouraged us to apply them in the field of water treatment, which will be discussed in forthcoming publications**.**

References

[1] J.-W. Ha , I. J. Park , S.-B. Lee and D.-K. Kim , *Macromolecules*, 2002, **35** , 6811 -6818
[2] R A Ramli, W A Laftah and S Hashim, RSC Advances, 2013, 3, 15543
[3] A. Aguiar, S. González-Villegas, M. Rabelero, E. Mendizábal, J. E. Puig, J. M. Domínguez and I. Katime, *Macromolecules* 1999, 32, 20, 6767–6771
[4] C. Pichot , D. Duracher , A. Elaissari and F. Mallet , *Polymer Preprints (American Chemical Society Division of Polymer Chemistry)*, 2000, **41** , 1026 -1027

[5] G. R. Hendrickson , M. H. Smith , A. B. South and L. A. Lyon , *Adv. Funct. Mater.*, 2010, **20** , 1697 -1712
[6] M A. Akl, A. M. Yousef, M A. Ibrahim and A M. Atta(2013) polymer international 62, (12), pages 1667–1677
[7] MA. Akl, AA. Sarhan, KR. Shoueir , A M. Atta, JDST, 2013, 34(10), 1399-1408
[8] M A Akl, A Atta, A M Youssef and M A Ibraheim, J Chromat Separation Techniq 2013, 4:5:185
[9] A Atta, M A Akl, A M Youssef and M A Ibraheim (2013)Adsorption Science & Technology, Vol. 31 No. 5, 397
[10] K R Shoueir, A Sarhan, A M Atta & M A Akl, Separation science & technology, 2016, Volume 51, Issue 10, Pages 1605-1617
[11] K R Shoueir, M A Akl, A A Sarhan & A M Atta, Applied Water Science, 2016 ,1-12,
[12] K R. Shoueir, A M. Atta, A A. Sarhan & M A. Akl, Environmental Technology, **2017 - 38 (8)**, 967-97
[13] L J Borthakura, D Dasb, S K. Doluib, Materials Chemistry and Physics, 124 (2010) 1182–1187
[14] M. Kawasumi, Journal of Polymer Science Part A: Polymer Chemistry, 2004, 42, 819-824.
[15] C. LeBaron, Z. Wang and T. J. Pinnavaia, Applied Clay Science, 1999, 15, 11-29.
[16] X. Fu and S. Qutubuddin, Polymer, 2001, 42, 807-813.
[17] K. A. Carrado, Applied Clay Science, 2000, 17, 1-23.
[18] Z. Tong and Y. Deng, Polymer, 2007, 48, 4337-4343.
[19] Huang and W. J. Brittain, Macromolecules, 2001, 34, 3255-3260.
[20] Sun, Y. Deng and Z. L. Wang, Macromolecular Materials and Engineering, 2004, 289, 288-295.
[21]M. Xu, Y. S. Choi, Y. K. Kim, K. H. Wang and I. J. Chung, Polymer, 2003, 44, 6387-6395.
[22]X. Huang and W. J. Brittain, Macromolecules, 2001, 34, 3255-3260.
[23]N. N. Herrera, J. M. Letoffe, J. L. Putaux, L. David and E. Bourgeat Lami, Langmuir, 2004, 20, 1564-1571.
[24] J. W. Kim, H. J. Choi and M. S. Jhon, (2000), Macromol. Symp. 155, 229–237
[25] T. Gopakumar, J. Lee, M. Kontopoulou and J. Parent, Polymer, 2002, 43, 5483-5491.
[26] M. T. López-López, A. Gómez-Ramírez, J. D. G. Durán and F. González-Caballero, Langmuir, 2008, 24, 7076-7084.
[27] L. Liang, J. Liu and X. Gong, Langmuir, 2000, 16, 9895-9899.
[28] M M. Sobeih, M. F. El-Shahat, A. Osman, M. A. Zaidb and M Y. Nassar , RSC Adv., 2020, 10, 25567–25585
[29] M. Y. Nassar, I. S. Ahmed and M. A. Raya, J. Mol. Liq., 2019, 282, 251–263.
[30] X. Tan, J. Hu, X. Zhou, S. Yu and X. Wang, Radiochimica Acta, 2008, 96, 487-495.
[31] R. Koswojo, R. P. Utomo, Y. H. Ju, A. Ayucitra, F. E. Soetaredjo, J. Sunarso and S. Ismadji, Applied Clay Science, 2010, 48, 81-86.
[32] S. Yang, D. Zhao, H. Zhang, S. Lu, L. Chen and X. Yu, Journal of hazardous materials, 2010, 183, 632-640.
[33] S. Sonawane, P. Chaudhari, S. Ghodke, M. Parande, V. Bhandari, S. Mishra and R. Kulkarni, Ultrasonics sonochemistry, 2009, 16, 351-355.
[34] B. Erdem, A. Özcan, Ö. Gök and A. S. Özcan, Journal of hazardous materials, 2009, 163, 418-426.
[35] F. Q. Zhang, Z. J. Guo, H. Gao, Y. C. Li, L. Ren, L. Shi and L. X. Wang, Polymer Bulletin, 2005, 55, 419-428.
[36] A. Li, A. Wang and J. Chen, Journal of Applied Polymer Science, 2004, 92, 1596-1603.
[37] T. Huang, H. Xu, K. Jiao, L. Zhu, H. R. Brown and H. Wang, Advanced Materials, 2007, 19, 1622-1626.
[38] J. Zhang and A. Wang, Reactive and Functional Polymers, 2007, 67, 737-745.
[39] E Kang, B Graczykowski, U Jonas, D Christie, L A. G. Gray, D Cangialosi, et al. Macromolecules. 2019 Jul 23; 52(14): 5399–5406.
[40] T. Hatakeyama and F. Quinn, Fundamentals and Applications to Polymer Science, Thermal Analysis, 1994